SLAC-PUB-1071
(EXP)
July 1972

A SPARK CHAMBER MEASUREMENT OF THE REACTIONS $\pi^{\pm} + p \rightarrow \rho^{\pm} + p$ at 15 GeV/c*

J. C. Pratt, W. T. Kaune, W. L. Lakin**, M. L. Perl,
E. W. Petraske***, J. Tenebaum† and W. T. Toner††

Stanford Linear Accelerator Center
Stanford University, Stanford, California

ABSTRACT

A new method, using spark chambers, for the study of the reactions $\pi^{\pm} + p \rightarrow \rho^{+} + p$ is described. The charged pion and both γ rays from the $\rho^{\pm}$ decay are detected. Differential and integrated cross sections ($\sigma_{\rho^+} = 50 \pm 9\ \mu b$, $\sigma_{\rho^-} = 47 \pm 9\ \mu b$) for $0.0 \leq |t| \leq 1.\ (GeV/c)^2$ and a laboratory momentum (p_{Lab}) of 15 GeV/c are presented. The momentum dependence of $\sigma_{\rho^{\pm}}$ is well fitted from 2.7 to 16 GeV/c by $\sigma = K p_{Lab}^{-n}$ with $n_{\rho^+} = 1.80 \pm .08$ and $n_{\rho^-} = 1.87 \pm .15$.

(Submitted to Physics Letters. Also submitted to the XVI International Conference on High Energy Physics, Batavia, Illinois, Sept. 6-13, 1972)

---

*Work supported by the U. S. Atomic Energy Commission

** Now at University of Birmingham, Birmingham B15 2TT, England

*** Now at Vanderbilt University, Nashville, Tennessee 37203.

†Now at State University of New York at Purchase, Purchase, New York 10577

†† Now at Rutherford High Energy Laboratory, Chilton, Didcot, Berkshire, England

In this letter we describe a new technique for studying the reactions

$$\pi^{\pm} + p \rightarrow \rho^{\pm} + p \qquad (1)$$

at high energy; and we present differential cross section measurements at 15 GeV/c obtained with this new technique. In this method, events belonging to this reaction are selected using optical spark chambers (a) to detect the $\pi^{\pm}$ and both γ rays from the decay sequence $\rho^{\pm} \rightarrow \pi^{\pm} + \pi^{o} \rightarrow \pi^{\pm} + \gamma + \gamma$, and (b) to detect the recoil proton if its kinetic energy exceeds 20 MeV. If the proton kinetic energy is less than 20 MeV, events belonging to this reaction are still selected with the aid of of an elaborate veto system which rejects contaminations from other final states.

This new technique offers two features to the experimenter who wishes to study these reactions without using the conventional bubble chamber technique. First, because this is a triggered spark chamber experiment, it is inherently capable of being used at higher energies where the cross sections of reactions (1) are very small. In fact, the technique is more easily applied at higher energies because as the energy increases, the relative geometric acceptance of the apparatus increases. Second, this same apparatus can, and has, been used to study the reaction

$$\pi^{-} + p \rightarrow \rho^{o} + n. \qquad (2)$$

This permits the extraction of the contribution of t-channel isoscalar exchange processes to reactions (1) and (2), all of the data coming from the same apparatus.

The apparatus is shown in Fig. 1. The pion beam, of either sign, was defined by the beam hodoscope (HD) with an outside veto counter (A_1, A_2). The liquid hydrogen target (HT) was 50 cm long and 2 cm diameter. A downstream veto counter (A_3) signaled the absence of an interaction. Counters (TV), constructed of alternate layers of lead and scintillator, covered the top and sides of the hydrogen target. These counters and a "window frame" of similarly constructed

counters (DV), downstream of the target, vetoed charged particles and γ rays outside of the acceptance of the experiment. Spark chamber (R), below the target, detected the recoil proton if $|t|^1$ was larger than .04 $(GeV/c)^2$. The lower section of this spark chamber provided a measurement of the energy, using range, to about 10% accuracy. Protons going toward the top and sides of the target were vetoed by the TV counters for $|t| > .08$ $(GeV/c)^2$.

The charged pion passed first through aluminum foil plates in two optical spark chambers (T_1, T_2). An array of 16 small scintillators (CT) between T_1 and T_2 determined the multiplicity of charged particles. The outer portions of 10 of the 13 T_2 plates were stainless steel, each .53 radiation lengths thick. These plates were used to detect γ rays, via their showers, which passed through the hole in the DV veto counters, but which were at too large an angle to be detected in chambers T_3 and T_4 as discussed below.

After leaving T_2, the charged pion entered the large momentum analyzing magnet (202cm high by 91cm wide, $\int Bd\ell$ = 26.5 kGm). Upon leaving the magnet the charged pion passed through optical spark chamber (T_3) with 7 aluminum foil plates and 10 thick plates and optical spark chamber (T_4) with 17 thick plates. This set of spark chambers and magnet yielded an average momentum resolution of $\pm$ 1.5%. The thick plates of chambers T_3 and T_4 each contained .44 radiation lengths of lead and .08 radiation lengths of aluminum. γ rays from the π^o were converted in these chambers and their showers detected by 16 scintillation counters (RG) between T_3 and T_4. Thus in a good event the charged pion track appeared in chambers T_1, T_2, T_3, and T_4; and showers from two γ rays appeared in chambers T_2 and/or T_3 and T_4. In addition a proton track might appear in chamber R if the proton's energy were sufficiently high. The trigger for pulsing the spark chambers and

taking a picture was designed to select events in the channel

$$\pi^{\pm} + p \rightarrow \pi^{\pm} + \pi^{o} + p \rightarrow \pi^{\pm} + \gamma + \gamma + p \qquad (3)$$

and to strongly discriminate against events with additional charged particles or γ rays.

Data was taken for equal lengths of time using alternately the π^+ and π^- beams at an average intensity of 3 pions per 1.4 microsecond accelerator pulse. The film was scanned for two γ ray events with one or more charged pion tracks and with or without a proton track. A rescan was done of these events on the measuring table. The overall, single pass, scanning and measuring efficiency was 73 ± 3%.

Events in which the proton was visible in chamber R were overconstrained in the conventional sense. If the proton stops in the range chamber, the requirement that both γ rays come from a π^o leads to the equivalent of a three-constraint fit, in bubble chamber terminology. If the proton passes out the bottom of the range chamber, we obtain the equivalent of a two constraint fit.

Events in which the proton was not visible in the range chamber because the proton energy was too small are called no-visible-proton events. These events were also overconstrained, but in a novel sense. The overconstraint, discussed in detail in the next two paragraphs, comes from the following two sources: (a) the electronic and optical (via the spark chambers) veto of events with multiplicities greater than that of reactions (3), and (b) the limit on the proton energy to less than 20 MeV if it is not visible in chamber R and does not pass into TV or DV.

a) All events with $0 \leq |t| \leq .04$ $(GeV/c)^2$ are no-visible-proton events. Events in the range $.04 \leq |t| \leq .08$ $(GeV/c)^2$ are visible proton events if the direction of motion of the proton is toward chamber R, otherwise they are no-visible-proton events (the TV counters veto all protons with $|t| > .08$ $(GeV/c)^2$). The veto counters and spark chamber surrounding the hydrogen target provided a 97% average

probability that a single charged particle or single γ ray leaving the target would be detected. Therefore the probability was very small that no-visible-proton events with charged particle or π^o multiplicities higher than that of channel (3) would be mistaken for the no-visible-proton event of channel (3). The largest source of contamination is events from the reactions

$$\pi^{\pm} + p \rightarrow \pi^{+} + n + \pi^{\pm} + \pi^{o}, \quad \pi^{o} + p + \pi^{\pm} + \pi^{o}$$

in which the $(\pi^{\pm} \pi^{o})$ invariant mass lies in the ρ mass range and the $(\pi^{+} n)$ or $(\pi^{o} p)$ invariant mass lies in the Δ (1238) mass range. This contamination was estimated to be $8 \pm 8\%$ and to be evenly distributed over the entire no-visible-proton t range.

b) Once the electronic and optical veto has eliminated additional charged and neutral pions in the no-visible-proton events as described in (a), the restriction of the proton kinetic energy to less than 20 MeV is a powerful constraint on the fitting since the difference between the three-momenta of the initial and final pions is severely limited.

In fitting the no-visible-proton events there is a two-fold ambiguity as to which γ ray has the higher energy. This introduces a two-fold ambiguity in the direction of the π^o and in the value of t. In many cases the restriction on the proton's kinetic energy resolved this ambiguity. However, in addition, all γ ray showers were studied to determine which γ-ray was of higher energy. This study resolved the ambiguity for most of the remaining events; Monte-Carlo studies indicated systematic effects were insignificant.

Our entire method of anlaysis of the no-visible-proton events was verified by studying the decay $K^{\pm} \rightarrow \pi^{\pm} + \pi^{o} \rightarrow \pi^{\pm} + \gamma + \gamma$ of K mesons in the beam. These decays are <u>three-constraint</u> fits. They allowed us to check the validity of our method of determining which γ-ray was of higher energy, to determine our resolution in

t of the no-visible-proton events, to measure the γ-ray conversion efficiency of our spark chamber, to check our calculation of the geometric acceptance, and to make sure that there were no asymmetries or other biases in the apparatus-either electronic or visual. In particular, these K decay studies showed that our determination of $|t|$ in the no-visible-proton events has an r.m.s. error of $\pm .007$ $(\mathrm{GeV/c})^2$, including effects from the π^o ambiguity.

To study reactions (1) 1756 events from both reactions were selected by the mass cut $665 \leq M_{\pi^\pm \pi^o} \leq 865$ MeV. Using these events we have calculated the differential cross sections by correcting for the acceptance of our apparatus and by fitting the mass spectrum to a relativistic Breit-Wigner formula ($\Gamma = 160$ MeV) plus a slowly varying background. This was done independently in each t bin and in each t bin the resonance dominated the mass spectrum. The average background which was subtracted was 6%.

The differential cross sections[2] for the reactions $\pi^\pm + p \rightarrow \rho^\pm + p$ are given in Fig. 2. The errors shown are purely statistical. There is an additional overall systematic uncertainty of $\pm 17\%$ which applies equally to both reactions. This uncertainty is the summation of various small uncertainties associated with the fitting and normalization procedures. We observe the expected strong forward peak in both reactions. $d\sigma/dt\ (\pi^\pm\ p \rightarrow \rho^\pm p)$ is in agreement in both shape and magnitude with a measurement[3] of that reaction carried out at 16 GeV/c in a hydrogen bubble chamber.

The integrated cross sections[4] ($\sigma_{\rho^\pm}$) for each reaction for $0 \leq |t| \leq 1.0\ (\mathrm{GeV/c})^2$ are

$$\sigma_{\rho^+} = 50 \pm 9\ \mu b$$

$$\sigma_{\rho^-} = 47 \pm 9\ \mu b.$$

The error here includes the $\pm 17\%$ overall systematic uncertainty previously discussed. Figure 3 presents a comparison of these results with previous

measurements[3, 5-10] at other energies. The line is a fit to these measurements of the form $\sigma = K\, p_{Lab}^{-n}$. We find $n_{\rho^+} = 1.80 \pm .08$ and $n_{\rho^-} = 1.87 \pm .15$. Comparisons of this data with $d\sigma/dt$ from reactions (2), isolation of the contribution of t-channel isoscalar exchange processes, and some theoretical interpretation is given in a subsequent paper[11].

We acknowledge with thanks the help of Dr. T. F. Zipf in the construction and operation of the experiment.

REFERENCES

1. Because of the high energy we do not distinguish between $t = 0$ and t_{min} since at the ρ mass $|t_{min}| = 0.00035$ $(GeV/c)^2$.
2. We have not included our data in the $0.000 \leq |t| \leq 0.015$ $(GeV/c)^2$ range on Fig. 2 because the error estimate in that bin may have to be enlarged to allow for a kinematic peculiarity which permits badly measured events to collect in the small t region of $0.000 \leq |t| \leq 0.00075$ $(GeV/c)^2$. The verification of the calculation of the error estimate awaits the completion of the analysis of sample data which we took at 8 GeV/c.
3. Aachen-Berlin-Bonn-CERN-Cracow-Heidelberg-Warsaw Collaboration Report, "Study of the Exchange Mechanisms in the Rho Production Reactions $\pi^{\pm} p \rightarrow \rho^{\pm} N$ at 16 GeV/c" (January 1972) unpublished.
4. We have chosen to emphasize the low and medium $|t|$ range, $0.0 \leq |t| \leq 1.0$ $(GeV/c)^2$, where we feel t-channel exchange mechanisms to be most valid.
5. J. P. Baton and G. Laurens, Nucl. Phys. B21, 551 (1970). We have extracted the cross section for $0 < |t| \leq 1.0$ $(GeV/c)^2$ using a relativistic Breit-Wigner shape ($\Gamma = 160$ MeV). We enlarged the error bars by a factor of 5 to allow for uncertainties in this procedure.
6. D. J. Schotanus et al., Nucl. Phys. B22, 45 (1970).
7. D. J. Crennell et al., Phys. Rev. Lett. 27, 1674 (1971).
8. W. Michael and G. Gidal, Phys. Rev. Lett. 28, 1475 (1972); G. Gidal, private communication.
9. M. Aderholz et al., Nucl. Phys. B8, 45 (1968).
10. S. L. Kramer et al., Particles and Nuclei 1, 131 (1970).
11. W. T. Kaune et al., "Isolation of Isoscalar Exchange in $\pi^{\pm} + p \rightarrow \rho^{\pm} + p$ at 15 GeV/c," SLAC (1972) to be published.

FIGURE CAPTIONS

1. Diagram of apparatus.
2. Differential cross sections for the reactions $\pi^{\pm} + p \rightarrow \rho^{\pm} + p$ at 15 GeV/c.
3. Integrated cross sections for $0.0 \leq |t| \leq 1.0$ $(GeV/c)^2$ of the reactions $\pi^{\pm} + p \rightarrow \rho^{\pm} + p$ as a function of laboratory momentum. Fitted line is $\sigma = Kp_{Lab}^{-n}$. For the following points we have extracted the integrated cross section for $0.0 < |t| < 1.0$ $(GeV/c)^2$: (a)[5], (b)[7], (d)[3], (e)[8], (f)[6], (g)[7], (h)[9], (m)[3]. For the following point we have plotted the total cross section quoted in the reference: (j)[10]. Points (c) and (k) are from this experiment.

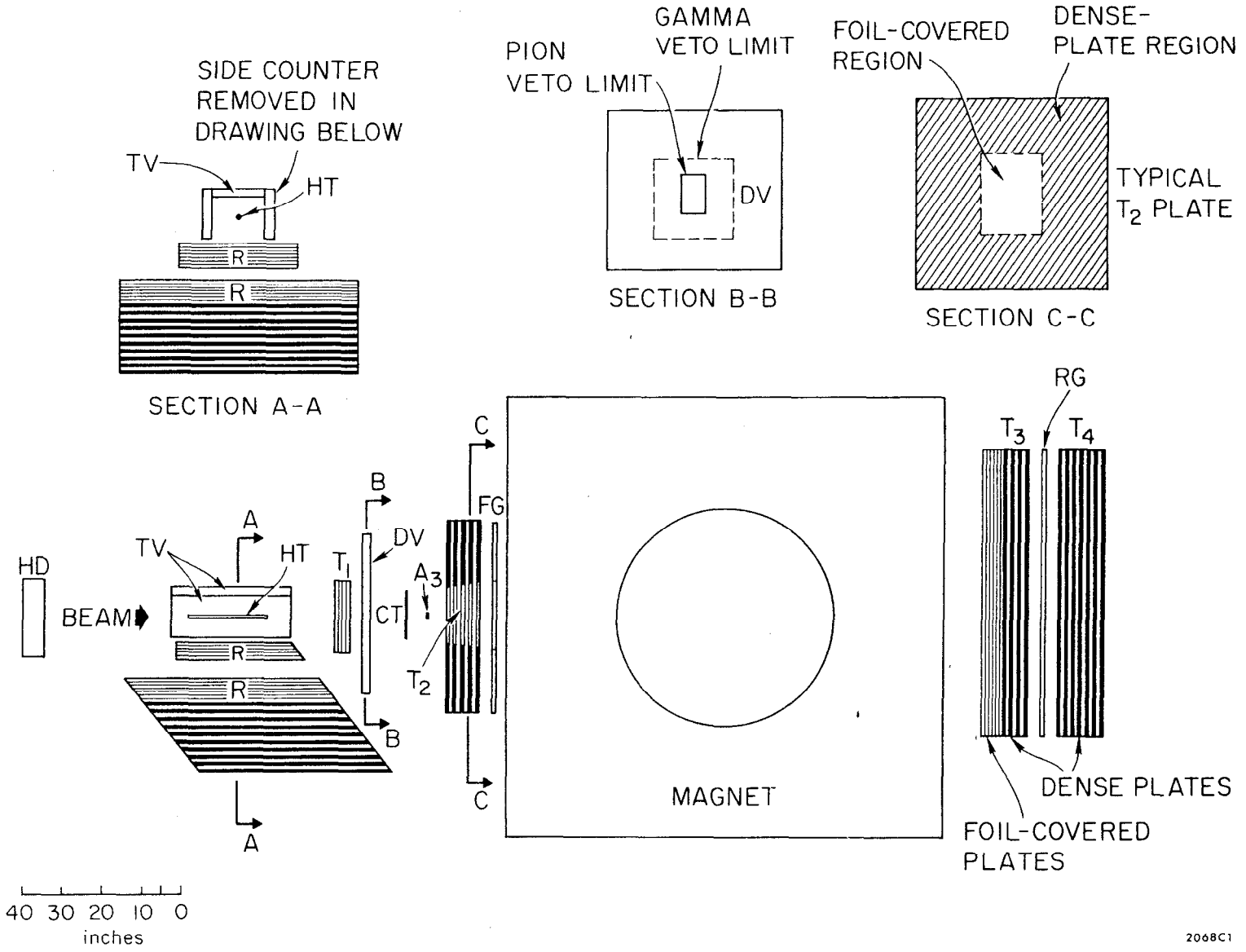
SIDE COUNTER
REMOVED IN
DRAWING BELOW
TV
HT
R
R
SECTION A-A
PION
VETO LIMIT
GAMMA
VETO LIMIT
DV
SECTION B-B
FOIL-COVERED
REGION
DENSE-
PLATE REGION
TYPICAL
T_2 PLATE
SECTION C-C
HD
BEAM
TV
HT
A
R
R
A
B
DV
T_1
CT
A_3
T_2
B
C
FG
C
MAGNET
RG
T_3
T_4
DENSE PLATES
FOIL-COVERED
PLATES
40 30 20 10 0
inches
2068C1

FIG. 1

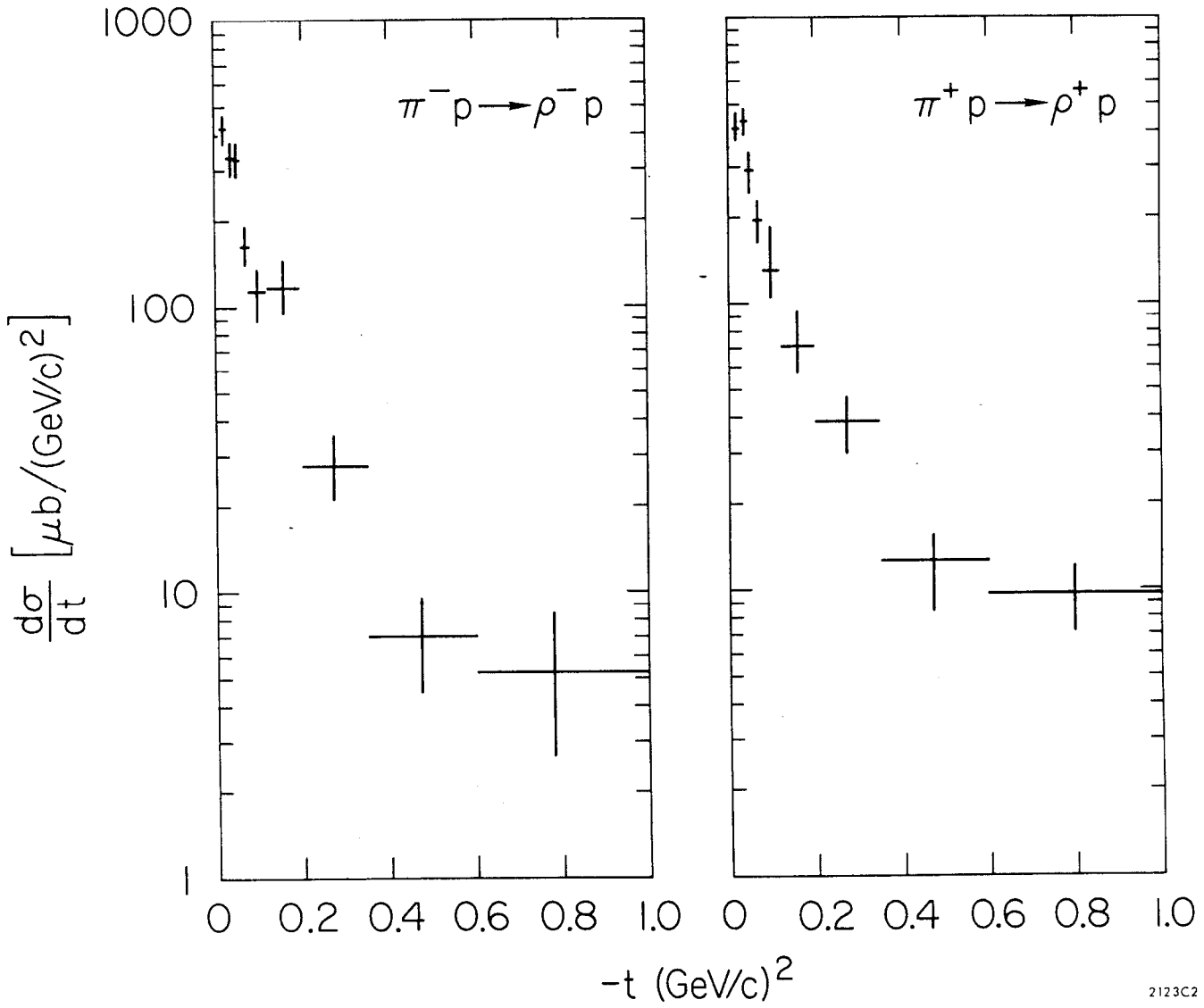
1000
100
10
1
$\frac{d\sigma}{dt}$ [μb/(GeV/c)^2]
$\pi^- p \rightarrow \rho^- p$
$\pi^+ p \rightarrow \rho^+ p$
0
0.2
0.4
0.6
0.8
1.0
$-t$ (GeV/c)^2
2123C2

FIG. 2

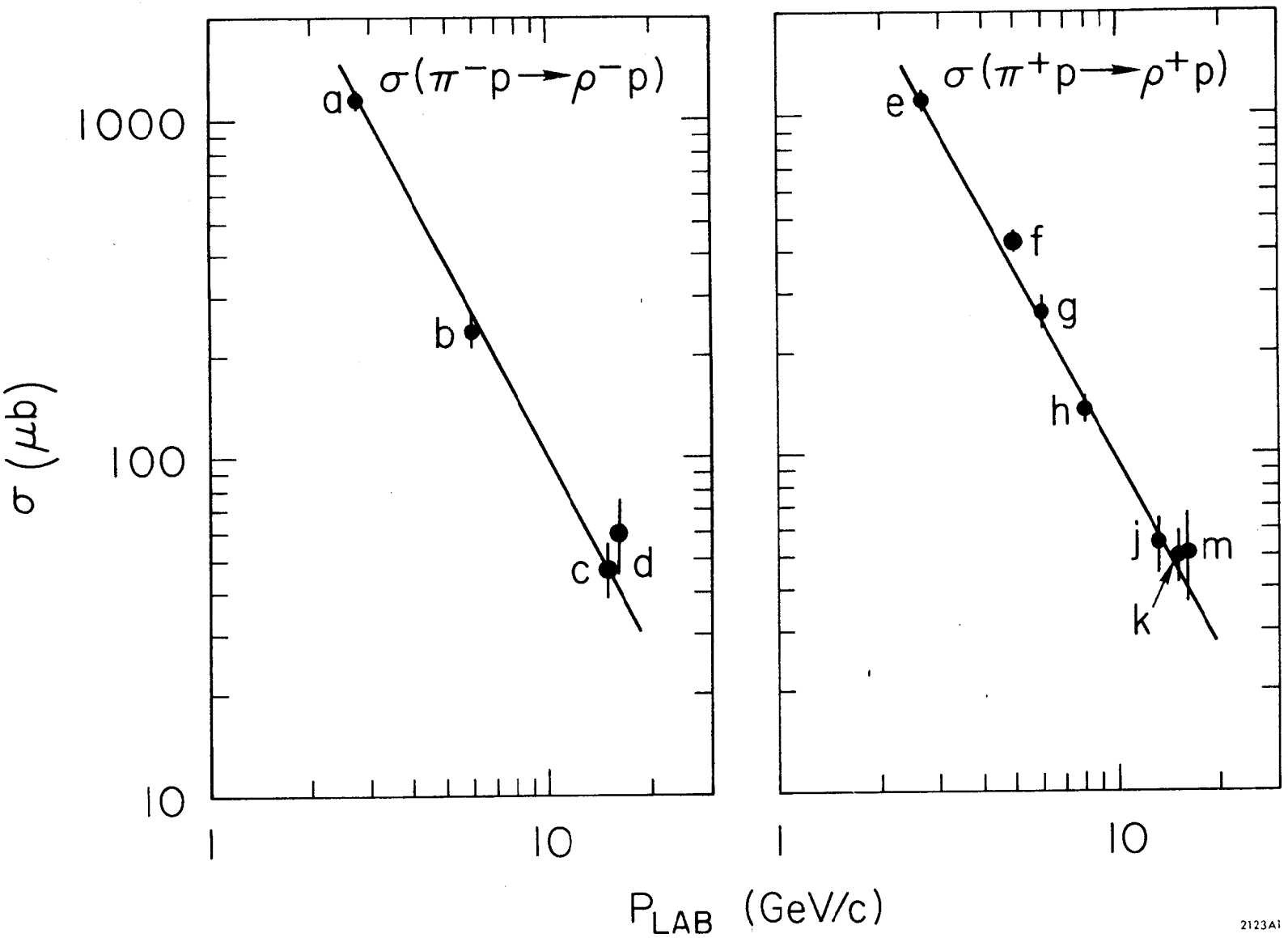
σ(π⁻p→ρ⁻p)
σ(π⁺p→ρ⁺p)
a
b
c
d
e
f
g
h
j
k
m
1000
100
10
σ (μb)
1
10
P_LAB (GeV/c)
2123A1

FIG. 3